Double-Perovskite Anode Materials Sr_2MMoO_6 (M = Co, Ni) for Solid Oxide Fuel Cells

Yun-Hui Huang,*[,†,#] Gan Liang,[‡] Mark Croft,[§,||] Matti Lehtimäki,[⊥] Maarit Karppinen,[⊥] and John B. Goodenough[†]

Texas Materials Institute, ETC 9.102, The University of Texas at Austin, Austin, Texas 78712 Department of Physics, Sam Houston State University, Huntsville, Texas 77341, Department of Physics, Rutgers University, Piscataway, New Jersey 08854, National Synchrotron Light Source, Brookhaven National Laboratory, Upton, New York 11973, Laboratory of Inorganic Chemistry, Department of Chemistry, Helsinki University of Technology, FI-02015 TKK, Finland, and State Key Laboratory of Materials Processing and Die and Mold Technology, School of Materials Science and Engineering, Huazhong University of Science and Technology, Wuhan, Hubei 430074, China

Received December 16, 2008. Revised Manuscript Received March 28, 2009

Double-perovskites Sr_2MMoO_6 (M = Co, Ni) have been investigated as anode materials for a solid oxide fuel cell. At room temperature, both Sr_2CoMoO_6 and Sr_2NiMoO_6 are tetragonal (*I4/m*). X-ray absorption spectroscopy confirmed the presence of Co^{2+}/Mo^{6+} and Ni^{2+}/Mo^{6+} pairs in the oxygen-stoichiometric compounds. The samples contain a limited concentration of oxygen vacancies in the reducing atmospheres at an anode. Reoxidation is facile below 600 °C; they become antiferromagnetic at low temperatures T_N = 37 and 80 K for M = Co and Ni, respectively. As an anode with a 300 μm thick $La_{0.8}Sr_{0.2}Ga_{0.83}Mg_{0.17}O_{2.815}$ electrolyte and $SrFe_{0.2}Co_{0.8}O_{3-\delta}$ as a cathode, Sr_2CoMoO_6 exhibited maximum power densities of 735 mW/cm^2 in H_2 and 527 mW/cm^2 in wet CH_4 at 800 °C; Sr_2NiMoO_6 shows a notable power output only in dry CH_4. The high performance of Sr_2CoMoO_6 in wet CH_4 may be due to its catalytic effect on steam reforming of methane, but some degradation of the structure that occurred in CH_4 obscures identification of the catalytic reaction processes at the surface. However, the stronger octahedral-site preference of Ni^{2+} versus Co^{2+} can account for the lower performance of the M = Ni anode.

Introduction

The solid oxide fuel cell (SOFC) is an electrochemical device that can be used for either stationary or mobile generation of electrical energy from a gaseous fuel. The conventional SOFC, which uses $Y_{2x}Zr_{1-2x}O_{2-x}$ (YSZ) as the electrolyte and a porous Ni−YSZ cermet anode, is commercially viable with pure H_2 or syngas as the fuel; but this anode is fouled by carbon deposition and sulfur poisoning when operated on natural gas.[1−3] Development of an anode material that can operate on natural gas would provide a cheaper, more convenient SOFC. For this application, oxides that are mixed oxide-ion/electron conductors (MIECs) in the reducing atmosphere at the anode have been under investigation.[3,4] The double- perovskite Sr_2MgMoO_6 is a promising MIEC with an excellent tolerance to sulfur that gives direct electrochemical oxidation in dry methane at 800 °C.[5,6] Moreover, La-doped Sr_2MgMoO_6 performs somewhat better on natural gas.[7] These results have prompted a study of other members of the Sr_2MMoO_6 family containing a 3d-block transition-metal M to investigate the role of the M cation.

The ordered double-perovskites $A_2BB'O_6$ have alternating $BO_{6/2}$ and $B'O_{6/2}$ corner-shared octahedra. Substitution at A or B sites can alter the cation valence and oxygen-vacancy concentration. As is well-known, cation valence and oxygen-vacancy concentration play important roles in the physical and electrochemical properties of the double perovskites.[8−11] In Sr_2MgMoO_6, Mg ions show unchanged divalence; only the valence of Mo ions changes from +6 to +5 with the introduction of oxygen vacancies. Co and Ni ions are multivalent; the evolution of cation valence and oxygen-vacancy concentration in Sr_2CoMoO_6 and Sr_2NiMoO_6 is more complicated than that in Sr_2MgMoO_6. In this paper, we have systematically explored the valence states and the

* To whom correspondence should be addressed. E-mail: huangyh@mail.hust.edu.cn.
† The University of Texas at Austin.
‡ Sam Houston State University.
§ Rutgers University.
|| Brookhaven National Laboratory.
⊥ Helsinki University of Technology.
Huazhong University of Science and Technology.

(1) McIntosh, S.; Gorte, R. J. *Chem. Rev.* **2004**, *104*, 4845.
(2) Sun, C. W.; Stimming, U. *J. Power Sources* **2007**, *171*, 247.
(3) Goodenough, J. B.; Huang, Y. H. *J. Power Sources* **2007**, *173*, 1.
(4) Atkinson, A.; Barnett, S.; Gorte, R. J.; Irvine, J. T. S.; McEvoy, A. J.; Mogensen, M.; Singhal, S. C.; Vohs, J. *Nat. Mater.* **2004**, *3*, 17.
(5) Huang, Y. H.; Dass, R. I.; Xing, Z. L.; Goodenough, J. B. *Science* **2006**, *312*, 254.
(6) Huang, Y. H.; Dass, R. I.; Denyszyn, J. C.; Goodenough, J. B. *J. Electrochem. Soc.* **2006**, *153*, A1266.
(7) Ji, Y.; Huang, Y. H.; Ying, J. R.; Goodenough, J. B. *Electrochem. Commun.* **2007**, *9*, 1881.
(8) Kobayashi, K. I.; Kimura, T.; Sawada, H.; Terakura, K.; Tokura, Y. *Nature (London)* **1998**, *395*, 677.
(9) Serrate, D.; De Teresa, J. M.; Ibarra, M. R. *J. Phys.: Condens. Matter* **2007**, *19*, 023201.
(10) García-Hernández, M.; Martínez, J. L.; Martínez-Lope, M. J.; Casais, M. T.; Alonso, J. A. *Phys. Rev. Lett.* **2001**, *86*, 2443.
(11) Huang, Y. H.; Karppinen, M.; Yamauchi, H.; Goodenough, J. B. *Phys. Rev. B* **2006**, *73*, 104408.

10.1021/cm8033643 CCC: $40.75
Published on Web 05/01/2009

electrochemical performances of the double-perovskites Sr_2MMoO_6 (M = Co, Ni) as anodes of a SOFC operating on dry and wet methane and on H_2.

Experimental Section

Sr_2CoMoO_6 and Sr_2NiMoO_6 samples were synthesized via a sol−gel method with stoichiometric $SrCO_3$ (Alirich, 99%), $(NH_4)_6Mo_7O_{24}\cdot 4H_2O$ (Fisher Scientific, assay MoO_3, 81.5%), and Co_3O_4 (Alfa, 99%) or NiO (Alfa, 99%) as the starting materials. $SrCO_3$ and Co_3O_4, NiO were first dissolved with diluted nitric acid and then mixed with $(NH_4)_6Mo_7O_{24}\cdot 4H_2O$. Ethylenediaminetetraacetic acid was added as a complexant to achieve a clear aqueous solution. The pH of the solution was adjusted to 9−10 with ammonia. The solution was evaporated on a hot plate to become a gel. The gel was first decomposed at 400 °C in air for 6 h and then calcined at 800 °C in air for 10 h. The calcined powder was pelletized and finally sintered at 1250 °C in air for 24 h to achieve a pure phase. Synthesis of other compounds, $La_{0.8}Sr_{0.2}Ga_{0.83}Mg_{0.17}O_{2.815}$, $SrCo_{0.8}Fe_{0.2}O_{3-\delta}$, and $La_{0.4}Ce_{0.6}O_{2-\delta}$, has been described elsewhere.[6]

The phase purity and the lattice parameters of the samples were checked by X-ray powder diffraction (XRD, Philips X-pert, Cu Kα radiation). The diffraction profiles were analyzed with a Rietveld refinement program, RIETAN 2000. Redox behaviors of the samples were investigated by thermogravimetric analysis (TGA, Perkin-Elmer Pyris 1 and Netzsch STA 449 C) in air and 5% H_2/Ar gas flows in the temperature range from room temperature to 1000 °C. In these TGA experiments, the amount of sample powder was ∼15 mg and the heating/cooling rate was either 2 or 10 °C/min. Micrographs were taken by a scanning electron microscope (SEM, Hitachi: S4500). Magnetization measurements were made with a superconducting quantum interference device (Quantum Design: MPMS-XL5). The conductivity was measured by a standard dc four-probe method with our own setup. The samples for conductivity measurement were polished into rectangular bars; Pt wire and Pt paste were used to make the four probes. Before measurement, the samples were reduced in 5% H_2/Ar in our own setup at 800 °C for 20 h to ensure formation of oxygen vacancies. Oxygen partial pressure was monitored with a Thermox CG1000 oxygen analyzer (Ametek).

The Mo L_3-edge, Ni K-edge, and Co K-edge X-ray absorption spectroscopy (XAS) measurements were performed in the fluorescence mode and on powdered samples on beamline X-19A at the National Synchrotron Light Source, Brookhaven National Laboratory. A double-crystal Si(111) monochromator was used. The XAS samples were prepared by dusting a fine powder of the samples onto scotch tape. In the case of the Ni and Co K-edge measurements, the X-ray beam transmitted through the samples allowed transmission-mode measurements along with edges of simultaneously run standards located on the down-beam side of the sample. The absolute energy calibration was set to the elemental edge (first inflection point). The relative energy scale was maintained to better than ±0.05 eV with the simultaneously run standards. In the case of the Mo L_3-edges, standards were run periodically in the sample sequence and the energy scale is better than ±0.1 eV.

Single SOFC test cells were fabricated by an electrolyte-supported technique with 300 μm thick $La_{0.8}Sr_{0.2}Ga_{0.83}Mg_{0.17}O_{2.815}$ (LSGM) as the electrolyte and $SrCo_{0.8}Fe_{0.2}O_{3-\delta}$ (SCF) as the cathode. The fabrication method of the single cell has been described in detail in our previous work.[6] A thin buffer layer of $La_{0.4}Ce_{0.6}O_{2-\delta}$ (LDC) between the anode and the electrolyte was used to prevent interdiffusion of ionic species between anode and electrolyte.[12] Pt gauze with a small amount of Pt paste in separate dots was used as a current collector at both the anode and cathode sides for ensuring contact. A double-layer sealing design was applied to the single cells. Before testing, the cells were exposed to 5% H_2/Ar for 20 h at 800 °C to reduce the anode and then purged with fuel gas for 2 h. The performance measurements were performed on an EG&G potentiostat/galvanostat model 273 with a homemade LabView program.

Table 1. Room-Temperature Lattice Parameters, Bond Lengths, Bond Angles, Density (d), Atom Occupancy (g_M), and Degree of Cationic Ordering (ξ) Obtained by Rietveld Refinement on XRD Patterns for Sr_2MMoO_6 (M = Co, Ni)

M	Co	Ni
space group	*I4/m*	*I4/m*
a (Å)	5.5726(3)	5.5463(2)
b (Å)	5.5726(3)	5.5463(2)
c (Å)	7.9575(5)	7.8933(3)
V (Å^3)	247.11(3)	242.81(1)
d (g/cm^3)	5.723	5.825
M−O1 (Å)	2.044(×2)	2.003(×2)
M−O2 (Å)	2.039(×4)	1.987(×4)
⟨M−O⟩ (Å)	2.041	1.993
Mo−O1 (Å)	1.935(×2)	1.953(×2)
Mo−O2 (Å)	1.935(×4)	1.951(×4)
⟨Mo−O⟩ (Å)	1.935	1.952
M−O1−Mo (deg)	180(×2)	180(×2)
M−O2−Mo (deg)	165.13(×4)	169.57(×4)
g_M	0.971(9)	0.979(5)
ξ	0.942	0.958
R_p (%)	7.45	5.54
R_{wp} (%)	10.46	7.23

Results and Discussion

The XRD patterns show that the samples were double-perovskite phases. Sr_2CoMoO_6 and Sr_2NiMoO_6 both have a tetragonal structure with space group *I4/m*. The lattice parameters, bond lengths, bond angles, and site occupancies obtained by Rietveld refinement are displayed in Table 1. The lattice cell volume of M = Co is larger than that of M = Ni; the mean bond length ⟨Co−O⟩ is longer than that of ⟨Ni−O⟩. The order is consistent with their ionic radii (sixfold coordination), i.e., Co^{2+} 0.745 Å (HS), Ni^{2+} 0.69 Å. The bond length ⟨Mo−O⟩ is shorter than that of ⟨M−O⟩ because Mo^{6+} (0.59 Å) and Mo^{5+} (0.61 Å) are both smaller than the ionic radii of the M cations. Reduction from 180° of the M−O−Mo bond angles is caused by a cooperative rotation of the $MO_{6/2}$ and $MoO_{6/2}$ octahedra; these rotations increase as the geometric tolerance factor $t = (r_A + r_O)/\sqrt{2}(r_B + r_O)$ decreases. The r_A, r_B, and r_O are respectively the room-temperature ionic radii of the A-site cation (ninefold coordination), the mean B-site ionic radius (sixfold coordination), and the oxide-ion radius (twofold coordination) with the Shannon[13] ionic radii. The t factors are 0.932 and 0.945 for M = Co and M = Ni, respectively. This assignment for the valence states places the Mo^{6+}/Mo^{5+} reduction potential above the M^{3+}/M^{2+} reduction potentials of M = Co and Ni.

The double-perovskite B-site cations generally exhibit some antisite disorder and antiphase boundaries. The value of the order parameter ξ can be calculated as $\xi = 2(g_M -$

(12) Huang, K. Q.; Goodenough, J. B. *J. Alloys Compd.* **2000**, *303−304*, 454.
(13) Shannon, R. D. *Acta Crystallogr.* **1976**, *A32*, 751.

0.5) from the refined occupancy of M ions at its correct site (g_M). Sr_2MMoO_6 with M = Co and Ni have a highly ordered structure, which is ascribed to the big difference in radius and valence between Co^{2+} and Mo^{6+}, Ni^{2+}, and Mo^{6+}.

The iodometric titration method can be used to determine directly the valence of some cations in the double perovskites.[14] According to their standard oxidation−reduction potential, Co^{3+} and Ni^{3+} can efficiently oxidize I^- to I_2. Therefore, we used this method to check the contents of Co^{3+} and Ni^{3+} ions. A weighed amount of double-perovskite powder was dissolved in diluted HCl aqueous solution and then excess KI was added. The purple iodine produced in situ was immediately titrated with a standard volumetric solution of sodium thiosulfate; starch was used as an indicator of the end point. The whole reaction can be expressed as follows:

$$2M^{3+} + 2I^- = I_2 + 2M^{2+} \quad (M = Co, Ni) \qquad (1)$$

$$2S_2O_3^{2-} + I_2 = 2I^- + S_4O_6^{2-} \qquad (2)$$

The percentages of Co^{3+}/Co and Ni^{3+}/Ni in the as-prepared Sr_2CoMoO_6 and Sr_2NiMoO_6 samples sintered in air were 6.7% and 4.2%, respectively.

We have shown in our previous work that some oxygen vacancies exist in the reduced Sr_2MgMoO_6.[5,6] Bernuy-Lopez and Marrero-López et al.[15,16] separately noted that reduction of Sr_2MgMoO_6 can give rise to a limited number of oxygen vacancies and hence to some lower Mo oxidation states than Mo^{6+}. Here, we focus on the temperature dependence of the oxygen vacancies in the as-prepared Sr_2CoMoO_6 and Sr_2NiMoO_6 samples in air and a 5% H_2/Ar atmosphere.

The perovskite structure does not accept interstitial oxygen. Therefore, the presence of M^{3+} species in the air-sintered samples requires the presence of some cation vacancies. Partial evaporation of some of the constituent metals during sintering at 1250 °C in air led to a cationic nonstoichiometry in the as-prepared samples.[17,18] We investigate how oxygen is lost and reincorporated on raising and lowering of the temperature with TGA. Since the Mo^{6+}/Mo^{5+} redox couple is at a higher energy than the M^{3+}/M^{2+} couples, reduction of the samples will, first, reduce the M^{3+} to M^{2+}. (*Note:* throughout we indicate formal valences on the cations, not the actual charges they carry.)

On heating in air, Figure 1A, both samples show the onset of weight loss at 300 °C and a step loss at 650 °C, corresponding to ca. 0.05 O atoms/f.u., that is shown to be irreversible in the case of M = Co. The M = Co sample also shows a second reversible weight-loss step at 900 °C; the M = Ni sample does not. This difference and the smaller oxidation of Ni^{2+} versus Co^{2+} reflects, we believe, a greater resistance to oxygen and Mo loss by the stronger preference

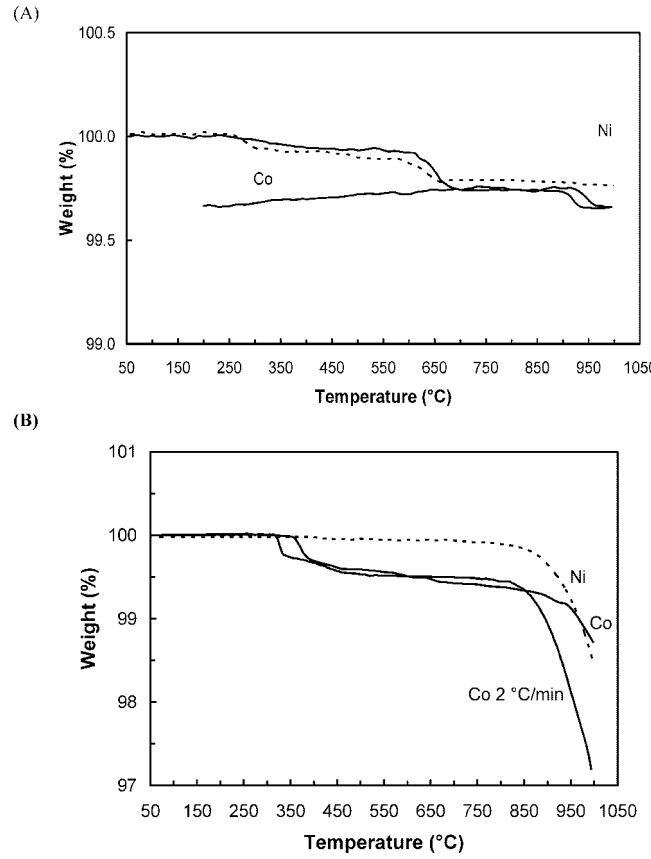

Figure 1. TG curves for Sr_2CoMoO_6 (solid line) and Sr_2NiMoO_6 (dotted line): (A) in air with a heating rate of 2 °C/min; (B) in 5% H_2/Ar with heating rates of 2 and 10 °C/min.

of Ni^{2+} for octahedral sixfold oxygen coordination. The step weight losses signal oxygen loss in a finite volume fraction, i.e., at defects. Oxygen vacancies trapped by formation of molybdyl (Mo═O) species at Mo-rich antiphase boundaries, for example, would provide an irreversible, finite oxygen loss. We postulate antisite Mo or Mo-rich antiphase boundaries are the operative defect since these would be common to both samples. The second step in the M = Co sample at 900 °C reflects, according to this reasoning, reversible trapping of an oxygen vacancy at some other defect associated with the M^{2+} ion since it does not occur in the M = Ni sample. Given the presence of Mo vacancies, we tentatively assign this step to trapping of oxygen vacancies at Co neighboring a Mo vacancy. A Co^{2+} ion at a Mo vacancy is stable in a lower oxygen coordination whereas the Ni^{2+} ion is much less stable in lower coordination.

Next, the TGA curves of Figure 1B were recorded on heating the as-prepared M = Co and M = Ni samples under a 5% H_2/Ar atmosphere, which resembles that at the anode of an operating SOFC. In this atmosphere, both samples begin to decompose above 800 °C where we have confirmed initiation of the reduction of MoO_3 with TGA measurements on MoO_3 in the same atmosphere (not shown), which contains Mo═O units. In 5% H_2/Ar, the step found at 650 °C in air does not appear with either sample. On the other hand, a significant reversible weight loss occurs in a step above 300 °C in the M = Co sample, but not in the M = Ni sample. Figure 2 shows that this weight loss in the M = Co sample is due to a reversible loss of oxygen. On heating in

(14) Vázquez-Vázquez, C.; Blanco, M. C.; López-Quintela, M. A.; Sánchez, R. D.; Rivas, J.; Oseroff, S. B. *J. Mater. Chem.* **1998**, *8*, 991.
(15) Bernuy-Lopez, C.; Allix, M.; Bridges, C. A.; Claridge, J. B.; Rosseinsky, M. J. *Chem. Mater.* **2007**, *19*, 1035.
(16) Marrero-López, D.; Martínez, J. P.; Ruiz-Morales, J. C.; Pérez-Coll, D.; Aranda, M. A. G.; Núnez, P. *Mater. Res. Bull.* **2008**, *43*, 2441.
(17) Huang, Y. H.; Lindén, J.; Yamauchi, H.; Karppinen, M. *Chem. Mater.* **2004**, *16*, 4337.
(18) Ivanov, S. A.; Eriksson, S. G.; Tellgren, R.; Rundlöf, H.; Tseggai, M. *Mater. Res. Bull.* **2005**, *40*, 840.

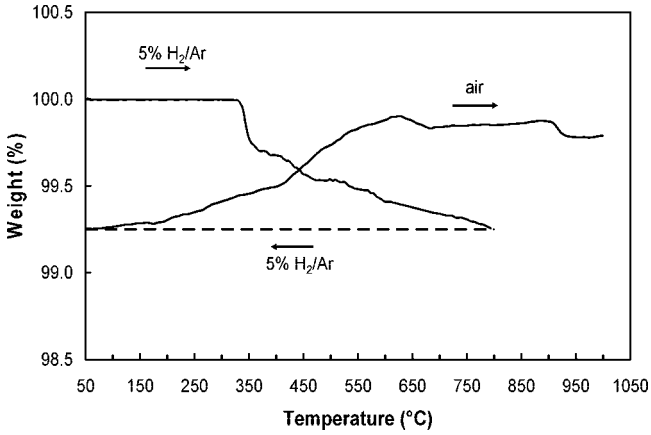

Figure 2. TG curves recorded for Sr_2CoMoO_6 with a heating rate of 2 °C/min first in 5% H_2/Ar up to 800 °C, and then for the same sample in air after cooling it rapidly down in 5% H_2/Ar (broken line).

air, a nearly complete regain of the weight lost occurs below 650 °C, and the weight-loss steps at 650 and 950 °C reappear. We therefore conclude that the small, irreversible weight loss in air above 350 °C in both samples, Figure 1, reflects reduction of M^{3+} to M^{2+}; it occurs more abruptly in the M = Ni sample because of the stronger octahedral-site preference of the Ni^{2+} ion. In the 5% H_2/Ar atmosphere, the M^{3+} ions would be reduced to M^{2+} already at room temperature and the vacancies introduced by this reduction are apparently trapped at the defects postulated to be Mo-rich antiphase boundaries. In the M = Co sample, the weight loss above 300 °C in 5% H_2/Ar would then represent a reduction of Mo^{6+} to Mo^{5+} by a reversible loss of oxygen that introduces mobile bulk oxygen vacancies. The stronger octahedral-site preference of Ni^{2+} inhibits further loss of oxygen in the 5% H_2/Ar atmosphere once the Ni^{3+} have been reduced to Ni^{2+} and the oxygen vacancies so introduced have been trapped. Heating the M = Co sample in air after reduction in 5% H_2/Ar reintroduces oxide ions that move, below 650 °C, to annihilate the trapped vacancies, vacancies that are again created on further heating above 650 °C.

In ref 19, a TGA curve was presented for H_2-reduced Sr_2CoMoO_6 to demonstrate its reoxygenation in air up to 800 °C. Even though the authors do not pay attention to the slight lowering of the curve after it reaches its maximum around 650 °C, it is clear that their TGA curve is highly consistent with the present data and conclusions.

The Mo L_3-edge, Ni K-edge, and Co K-edge XAS measurements were performed to confirm the cation valences. Since a simultaneous standard was not possible at the low energies of the Mo-L_3 edges, possible standards were run periodically in the sequence of samples and the relative energy was ±0.1 eV or better. In view of the low energy and strong "white line" *p*-to-*d* transition at the Mo-L_3 edge self-absorption, degradation/rounding of the absorption edge peaks in the fluorescence mode was unavoidable. Here the "white line" (WL) terminology is conventional and refers to an atomic-like dipole transition into empty states that typically manifests a sharply peaked near-edge structure; in

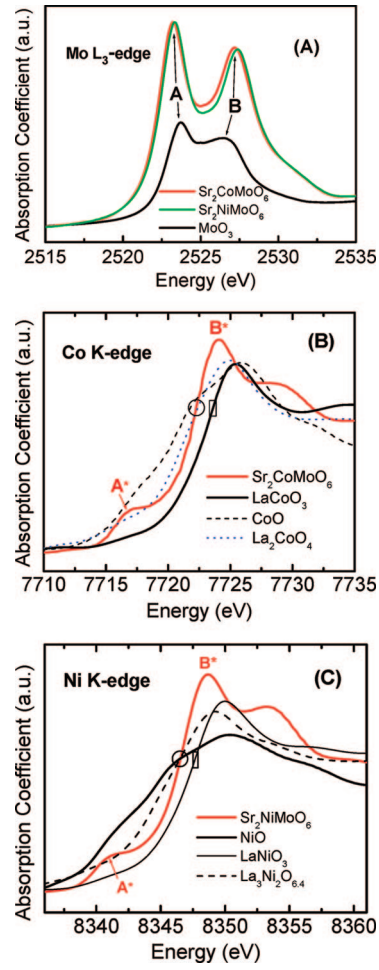

Figure 3. (A) Mo L_3-edge spectra for Sr_2MMoO_6 samples (M = Co, Ni) and standard MoO_3; (B) Co K-edge spectra for Sr_2CoMoO_6 and standards $LaCoO_3$, La_2CoO_4, and CoO; (C) Ni K-edge spectra for Sr_2NiMoO_6 and standards $LaNiO_3$, $La_3NiO_{6.4}$, and NiO.

prior years it left a white-line streak on photographic film.[20,21] As is routinely done, the spectra presented in this study had a linear background subtracted (determined over a ca. 80 eV interval below the edge) and were normalized to unity absorption step height across the edge. Here an average of the data in the 50−200 eV range above the edge was used to set the normalization value.

The L_3 near-edge WL features of 4d transition-metal compounds are due to transitions from the 2p to 4d states of the transition metal (such as Mo). In an octahedral ligand field, the d states of Mo^{6+} are split into a sixfold-degenerate t_{2g} ground state below a fourfold-degenerate e_g state. In Figure 3a the L_3-edge WL features of the octahedrally coordinated compounds Sr_2CoMoO_6 and Sr_2NiMoO_6 are shown in comparison with the spectra of another octahedrally coordinated compound, MoO_3. The A and B features are associated, respectively, with the t_{2g} and e_g final states of the octehedrally coordinated compounds. It should also be noted that the relative intensity of the A feature decreases as the number of empty t_{2g} states decreases (i.e., as the

(19) Okamoto, H.; Fjellvåg, H.; Yamauchi, H.; Karppinen, M. *Solid State Commun.* **2006**, *137*, 522.

(20) Wei, P. S. P.; Lytle, F. W. *Phys. Rev. B* **1979**, *19*, 679.

(21) Jeon, Y.; Jisrawi, N.; Liang, G.; Lu, F.; Croft, M.; Mclean, W. L.; Hart, D. L.; Stoffel, N. G.; Sun, J. Z.; Geballe, T. H. *Phys. Rev. B* **1989**, *39*, 5748.

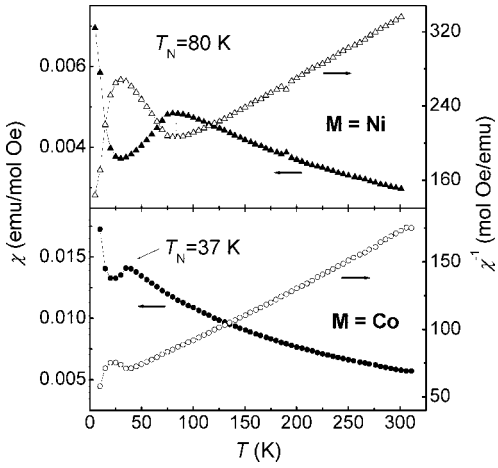

Figure 4. Magnetic susceptibility χ and reciprocal susceptibility χ^{-1} for the as-prepared Sr_2MMoO_6 (M = Co, Ni) samples.

electron count increases or valence decreases). Thus, the relative intensity ratio of the A to B features, I_A/I_B, can be used to track the d-electron/hole count in such Mo compounds; i.e., a higher I_A/I_B usually corresponds to a higher Mo valence.

The double-peak features A and B in Figure 3A are seen in all spectra and can be attributed to the $2p \rightarrow 4d(t_{2g})$ and $2p \rightarrow 4d(e_g)$ transitions, respectively. Since such double-peak features could have different widths for different compounds, it is more reliable to use the centrum or mean energy E_m (or characteristic energy[22,23]) instead of the edge energy (defined as the inflection point of the rising part of the edge) to estimate the Mo valence. The values of E_m estimated for these three spectra are almost identical (2525.5 eV), supporting the belief that the values of the Mo valence are nearly the same for these three compounds. The very close Mo valence in these three compounds indicates that Ni and Co are predominantly in the divalent state like that for Mg. To confirm this deduction, we show the Co and Ni K-edges of the Sr_2MMoO_6 compounds with M = Co and Ni, respectively, in Figure 3B,C, along with selected spectra of known formal valence standards: $LaM^{3+}O_3$, $M^{2+}O$, $La_3Ni_2O_{6.4}$, and $La_2Co^{2+}O_4$. The features *A** and *B** labeled on the spectra of the Sr_2MMoO_6 compounds are similar to what has been observed in the Ni K-edges of divalent nickel perovskite compounds $La_{2-x}Sr_xNiO_4$ ($0 \le x \le 0.2$)[24] and can be assigned to the transitions from the M 1s state to the final 4p states with different 3d electron-ligand hole configurations and orbital orientations. The Sr_2MMoO_6 compounds have chemical shifts for all the cations (see circles) consistent with a valence close to 2+ and shifted well down in energy from the 3+ (see rectangle) standard.

The magnetic susceptibility of the as-prepared Sr_2MMoO_6 samples was measured to check their electron configuration. Figure 4 displays the temperature dependence of the magnetic susceptibility χ and reciprocal susceptibility χ^{-1} for Sr_2MMoO_6 with M = Co and Ni. They both show a long-range-ordered antiferromagnetic state at low temperature. The Néel temperature T_N values are 37 and 80 K for M = Co and Ni, respectively. In the double-perovskite structure, the magnetically active M^{2+} ions are separated by magnetically neutral Mo^{6+} ions. The exchange interactions propagate through the intervening MoO_6 octahedra; therefore, a relatively high level of covalent bonding is expected within the M−O−Mo−O−M pathways. The variation of the T_N values depends primarily on the inverse of the energy separating the M^{3+}/M^{2+} and M^{2+}/M^{+} redox energies; the correlation energy U for Co^{2+} is larger than the charge-transfer gap Δ for Ni. Interestingly, with reduction of the air-sintered Sr_2CoMoO_6 sample in 5% H_2/Ar or H_2 at 800 °C for 10 h, the reduced sample exhibits a spin-glass ferromagnetism in the measured temperature range from 5 to 380 K. A similar phenomenon was also observed by Viola et al.[25] in oxygen-deficient $Sr_2CoMoO_{6-\delta}$ with a Curie temperature T_C = 350−370 K. The observed spin-glass ferromagnetism in $Sr_2CoMoO_{6-\delta}$ comes from a ferromagnetic superexchange between Co^{2+} ($3d^7$) and Mo^{5+} ($4d^1$) moments in the cation-ordered regions with antiferromagnetic M^{2+}−O−M^{2+} interactions across antiphase boundaries and at antisite M^{2+}.

A good fitting with the Curie−Weiss law is observed above T_N in the $\chi^{-1}-T$ curves for M = Co and Ni. The linear fitting above 200 K gives an effective paramagnetic moment (μ_{eff}) of 4.34(2) and 3.51(1) μ_B/f.u. for M = Co and M = Ni, respectively. For Sr_2CoMoO_6, the measured μ_{eff} is higher than the spin-only 3.87 μ_B for Co^{2+} ions. The measured μ_{eff} for Sr_2NiMoO_6 is also high relative to the predicted spin-only 2.83 μ_B for Ni^{2+} ions. Interpretation of the discrepancies between measured and spin-only μ_{eff} values is made complicated by the existence of antiphase boundaries where short-range magnetic order may occur above the T_N for the ordered regions.

Conductivity data taken above 350 °C while heating in different atmospheres are shown in Figures 5 and 6 for nominal $Sr_2CoMoO_{6-\delta}$ and $Sr_2NiMoO_{6-\delta}$, respectively. The conductivity above 350 °C is dominated by electrons on the Mo^{6+}/Mo^{5+} couple given the much lower mobility of the oxygen vacancies. The as-prepared M = Co sample gave positive thermoelectric power at room temperature showing that the conduction was by holes in the Co^{3+}/Co^{2+} couple (see Figure S4 in the Supporting Information), but the Co^{3+} are all reduced to Co^{2+} above 350 °C. In air, the $\log(\sigma T)$ vs T^{-1} curves for M = Co, Figure 5B, are linear below 650 °C, but the curve deviates to higher conductivity above 650 °C where the TGA curves of Figure 1A show a step. Electrons would be on Mo^{5+} coordinated by an oxygen vacancy, but trapping of oxygen vacancies at Mo=O species would release electrons to the matrix. The M = Ni sample in air had a larger resistivity with a nonlinear Arrhenius behavior below 650 °C, consistent with a small step in the TGA curve near 500 K and a saturation of the number of charge carriers.

(22) Alp, E. E.; Goodman, G. L.; Soderholm, L.; Min, S. M.; Ramanathan, R.; Shenoy, G. K.; Bommannavar, A. S. *J. Phys.: Condens. Matter* **1989**, *1*, 6463.
(23) Liang, G.; Yao, Q.; Zhou, S.; Katz, D. *Physica C* **2005**, *424*, 107.
(24) Sahiner, A.; Croft, M.; Guha, S.; Perez, I.; Zhang, Z.; Greenblatt, M.; Metcalf, P. A.; Jahns, H.; Liang, G. *Phys. Rev. B* **1995**, *51*, 5879.
(25) Viola, M. C.; Martínez-Lope, M. J.; Alonso, J. A.; Velasco, P.; Martínez, J. L.; Pedregosa, J. C.; Carbonio, R. E.; Fernández-Díaz, M. T. *Chem. Mater.* **2002**, *14*, 812.

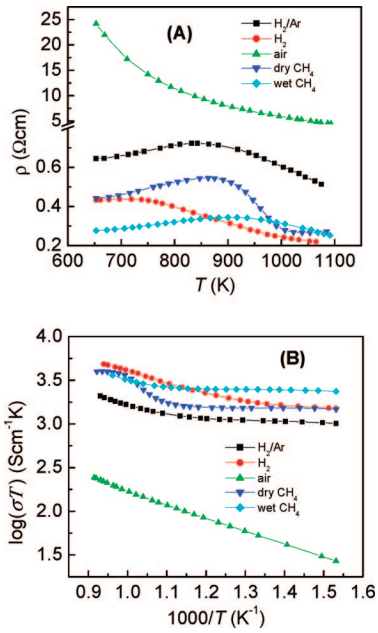

Figure 5. (A) Temperature dependence of resistivity (ρ) and (B) Arrhenius plots of $\log(\sigma T)$ vs T^{-1} for Sr_2CoMoO_6 in different atmospheres. The oxygen pressure pO_2 is around 10^{-18}, 10^{-19}, and 10^{-20} atm in CH_4 (dry or wet), 5% H_2/Ar, and H_2, respectively.

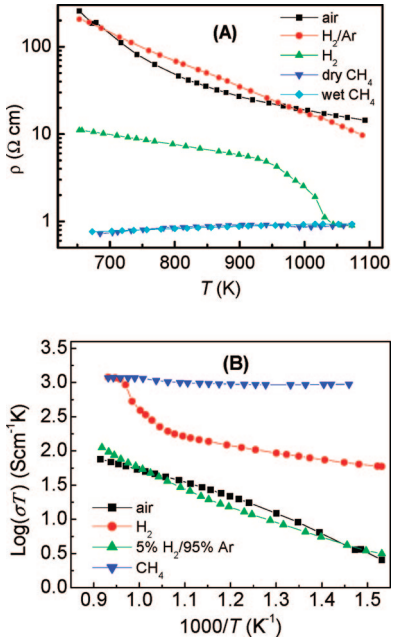

Figure 6. (A) Temperature dependence of resistivity (ρ) and (B) Arrhenius plots of $\log(\sigma T)$ vs T^{-1} for Sr_2NiMoO_6 in different atmospheres. The oxygen pressure pO_2 is around 10^{-18}, 10^{-19}, and 10^{-20} atm in CH_4 (dry or wet), 5% H_2/Ar, and H_2, respectively.

After reduction in 5% H_2/Ar for 20 h at 800 °C, the resistivity of the M = Co sample in that atmosphere shows a broad maximum near 650 °C where the TGA curve in air shows a step that we have postulated to be associated with formation of Mo═O species that trap oxygen vacancies. Since the system was carefully sealed so as to prevent leakage from air, the partial pressure of oxygen in the gas was extremely low ($pO_2 = 10^{-19}$ atm). Mo^{5+} ions would be trapped at oxygen vacancies unless formation of Mo═O species released the electrons. Nevertheless, at least half of the electrons introduced by the oxygen vacancies would be

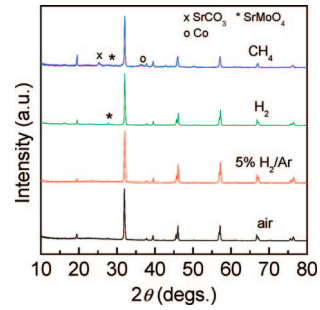

Figure 7. XRD patterns for air-sintered Sr_2CoMoO_6 after being reduced in 5% H_2/Ar, H_2, and CH_4 at 800 °C for 20 h.

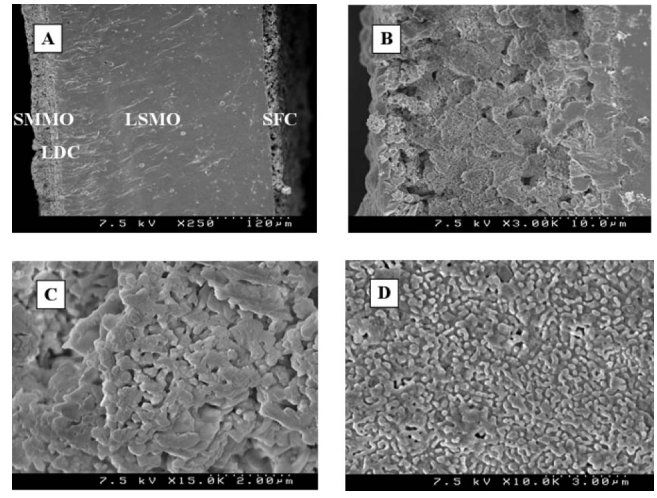

Figure 8. SEM images for the cell with the Sr_2CoMoO_6 anode: (A) cross section of the cell configuration, (B) section between LSGM and LDC buffer layer, (C) the surface of the Sr_2CoMoO_6 anode, and (D) the cathode SCF.

free to reduce the Co^{3+} to Co^{2+} or to move on the Mo in sixfold oxygen coordination. Although a small fraction of metallic cobalt or nickel was found in the XRD data of the samples after reduction in 5% H_2/Ar at 800 °C for 20 h (see Figure 7), this fraction was too small to percolate through the sample. Therefore, the grain conductivity can be assumed to be dominated by transfer of electrons from Mo^{5+} to Mo^{6+} octahedral sites. This assumption is supported by the increase in conductivity above 600 °C, which could be due to excitation of electrons from Co^{2+} to Mo^{6+} or, more likely, by release above 600 °C of electrons trapped at fivefold-coordinated Mo═O. The increase in resistivity with temperature below 600 °C is more problematic; but the motional enthalpy of polaronic conduction may increase with temperature or the grain-boundary contribution to the conductivity may be dominant at lower temperatures. An analogous increase in the conductivity of the M = Ni sample above 600 °C is also apparent.

The double-perovskite samples were tested as anode materials in SOFCs having a 300 μm thick LSGM electrolyte and $SrFe_{0.2}Co_{0.8}O_{6-\delta}$ cathode. Figure 8 shows SEM images for the single cell with Sr_2CoMoO_6 (SCMO) as the anode after operating in H_2 and CH_4. A clear cross section of the cell configuration can be seen in Figure 8A. Estimated from the SEM images, the thicknesses of the LSGM, SCMO, LDC, and SCF layers are 310, 26, 8, and 20 μm, respectively. The LDC buffer layer obviously exists between LSGM and

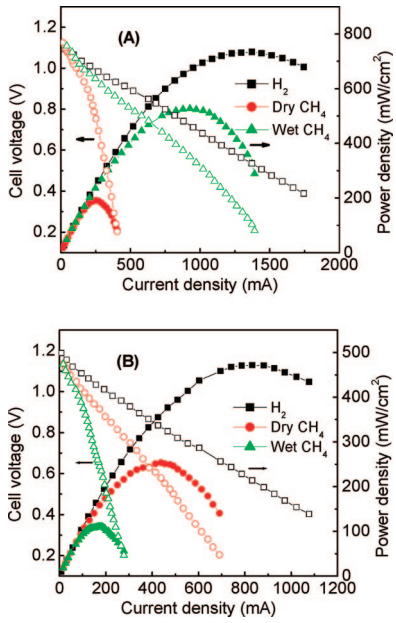

Figure 9. Power density and cell voltage as functions of current density at 800 °C in H_2, dry CH_4, and wet CH_4 for (A) Sr_2CoMoO_6 and (B) Sr_2NiMoO_6.

SCMO, which efficiently prevents a diffusion reaction between the anode and the electrolyte. Both anode and cathode layers are porous, which favors transfer of oxygen, fuel gas, and exhaust products.

Power density and cell voltage as functions of current density at 800 °C in H_2, dry CH_4, and wet CH_4 for cells with Sr_2MMoO_6 (M = Co and Ni) anodes are presented in Figure 9. In H_2, Sr_2CoMoO_6 exhibits a maximum power density (P_{max}) of 735 mW/cm^2 at a current density of 1380 mA/cm^2, almost comparable with Sr_2MgMoO_6.[5] In wet CH_4 (containing 3% H_2O), P_{max} reaches as high as 527 mW/cm^2 at a current density of 920 mA/cm^2, which is higher than that of Sr_2MgMoO_6. The Sr_2CoMoO_6 anode showed a remarkable electrochemical performance in H_2 and wet CH_4, but its power density in dry CH_4 was only 186 mW/cm^2, which is much lower than that in wet CH_4. Sr_2NiMoO_6 showed only a notable power output in dry CH_4.

We used power cycles to test the stability of the anodes in different fuels. Figure 10 shows the maximum power density as a function of cycle number for the Sr_2MMoO_6 (M = Co and Ni) anodes at 800 °C in H_2, dry CH_4, and wet CH_4. Each cycle was run from OCV (open circuit voltage) to 0.2 V and back to OCV, which took 20 min. A total of 50 cycles, i.e., 1000 min, was carried out for each anode. We define $P_{max,1}$ as the maximum power density for the first cycle and $P_{max,50}$ for the 50th cycle. Power loss was calculated by $(P_{max,1} - P_{max,50})/(P_{max,1}) \times 100\%$. Power loss over 50 cycles in H_2 is 6.3% and 6.8% for M = Co and M = Ni, respectively. In dry CH_4, Sr_2CoMoO_6 shows a $P_{max,1}$ of 186 mW/cm^2 and a power loss over 50 cycles of 24.2%; Sr_2NiMoO_6 shows a higher $P_{max,1}$ of 273 mW/cm^2 but a more rapid power loss over 50 cycles of 43.2%. In wet CH_4, Sr_2CoMoO_6 exhibits a large $P_{max,1}$ of 527 mW/cm^2, but the P_{max} value drops to 368 mW/cm^2 after 50 cycles, a 30.2% loss.

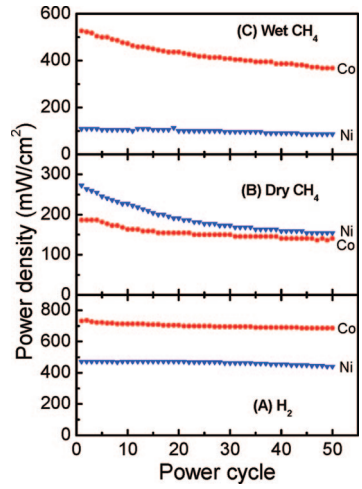

Figure 10. Maximum power density (P_{max}) as a function of power cycle for various anodes Sr_2MMoO_6 (M = Co and Ni) at 800 °C in H_2, dry CH_4, and wet CH_4.

The higher power output with H_2 fuel for the M = Co sample is consistent with its higher concentration of oxygen vacancies and higher electronic conductivity, which we believe to be the result of the stronger octahedral-site preference of the Ni^{2+} ions. From Figure 10, we can see that both Sr_2CoMoO_6 and Sr_2NiMoO_6 anodes run stably over power cycling in H_2, which can be ascribed to their stable phases in H_2. The XRD pattern in Figure 7 has typically shown that Sr_2CoMoO_6 is almost pure after being reduced at 800 °C in H_2 for 20 h.

The performances are quite different for Sr_2CoMoO_6 and Sr_2NiMoO_6 in dry and wet methane. Sr_2NiMoO_6 shows a higher power in dry CH_4, demonstrating that M = Ni favors the main process for direct oxidation of methane. The reaction can be expressed as

$$CH_4 + 4O^{2-} = CO_2 + 2H_2O + 8e^- \quad (3)$$

The O^{2-} ions are created in the cathode and transported through the electrolyte from the cathode. Sr_2CoMoO_6 exhibits a much higher power in wet CH_4, indicating a preferential reaction pathway on the anode through steam reforming of methane:

$$CH_4 + H_2O = CO + 3H_2 \quad (4)$$

We should take into account the catalytic effect of Sr_2CoMoO_6 on the above reformer reaction. Metallic Co was observed in Sr_2CoMoO_6 exposed to CH_4 (see the XRD patterns in Figure 7). Moreover, Co has been found to have high catalytic activity for the reforming of methane.[26,27] Therefore, it is reasonable to propose that the high performance for Sr_2CoMoO_6 in wet CH_4 fuel is due to the catalytic effect of surface Co^0 on the reformer reaction. Metallic Ni can also act as a catalyst for steam reforming of CH_4,[28] but the power density of Sr_2NiMoO_6 is lower than that of Sr_2CoMoO_6 in wet CH_4. We note that Ni easily induces formation of graphitic carbon on the catalyst, which causes

(26) Lucrédio, A. F.; Assaf, E. M. *J. Power Sources* **2006**, *159*, 667.
(27) Profeti, L. P. R.; Ticianelli, E. A.; Assaf, E. M. *Fuel* **2008**, *87*, 2076.
(28) Laosiripojana, N.; Assabumrungrat, S. *J. Power Sources* **2007**, *163*, 943.

catalytic deactivation and blockage of the reactor.[27] In addition, after exposure of the sample to CH_4, a tiny amount of $SrCO_3$ and $SrMoO_4$ also became visible in the XRD data (Figure 7). $SrCO_3$ and $SrMoO_4$, which would be on the surface of the anodes, may block the catalytic pathways for reforming of the fuel. These impurities would increase with operation time and may be the reason why the power density in CH_4 drops rapidly over cycling in Figure 10.

Conclusions

Magnetic, structural, and XAS data show the existence of Co^{2+}/Mo^{6+} and Ni^{2+}/Mo^{6+} pairs in the double-perovskites Sr_2MMoO_6. The Mo^{6+}/Mo^{5+} reduction potential is low enough to accept electrons from H_2 and CH_4, thus allowing dissociative chemisorption of the fuel. Moreover, displacement of a Mo^{6+} or a Mo^{5+} ion within an octahedral site to form a stable Mo═O species would trap oxygen vacancies in Mo-rich antiphase boundaries and release electrons trapped at oxygen vacancies; also, Mo═O species may favor reaction of the fuel with a surface oxide ion by lowering its acidity and energy for desorption of the oxidized reaction product. Polaronic conduction on the mixed-valent Mo^{6+}/Mo^{5+} array allows transfer of the electrons from the surface reaction to the current collector, and bulk oxygen vacancies allow transfer of O^{2-} ions from the oxide-ion electrolyte to the anode surface to replenish the surface oxygen that is lost. In methane, the rate-limiting processes are the chemical reactions occurring at the surface of the anode, but the dominant processes are obscured by the exolution onto the anode surface of Co or Ni and $SrCO_3$ with $SrMoO_4$ in the reducing atmosphere at the anode.

Acknowledgment. We thank the Robert A. Welch Foundation, Houston, TX, for support of this work. The work at Sam Houston State University (SHSU) was supported by the National Science Foundation under Grant No. CHE-0718482 and an award from Research Corporation. M.K. acknowledges financial support from the Academy of Finland (Decision Nos. 110433 and 116254). Y.H.H. acknowledges support from the National Science Fund for Distinguished Young Scholars of China (No. 50825203).

Supporting Information Available: Rietveld refinement of XRD patterns, magnetic susceptibility, thermoelectric power, and the average activation energy of electronic conduction for the anode materials.This material is available free of charge via the Internet at http://pubs.acs.org.

CM8033643